# Targeted delivery of tungsten oxide nanoparticles for multifunctional anti-tumor therapy *via* macrophages†

Bin Zheng,[‡a] Yang Bai,[‡b] Hongbin Chen,[a] Huizhuo Pan,[a] Wanying Ji,[a] Xiaoqun Gong,[a] Xiaoli Wu,[a] Hanjie Wang*[a] and Jin Chang*[a]

[a] School of Life Sciences, Tianjin University, 92 Weijin Road, Nankai District, Tianjin 300072, China. E-mail: wanghj@tju.edu.cn, jinchang@tju.edu.cn. Tel: +86-22-27403906.

[b] Department of Stomatology, Tianjin Medical University General Hospital, Tianjin, China.

† Electronic supplementary information (ESI) available. See DOI:

‡ Both authors contributed equally to this work.

**Abstract**

Tumor-associated macrophages are highly versatile effector cells that have been used in targeting to kill tumor cells. Herein, the macrophages as cell-based biocarriers can be used to targeted delivery of photothermal reagents for promoting the efficiency of killing tumor cells by activating the anti-tumor immune response and photothermal therapy (PTT). In this design, macrophages could phagocytosis tumor cells and activate the anti-tumor immune response by secreting plenty of cytokines. Meanwhile, to improve the tumor killing effect and track the collaborative therapy system *in vivo*, a novel nanoplatform based on tungsten oxide ($W_{18}O_{49}$, WO) nanoparticles and fluorescent dyes loaded in polylactic-co-glycolic acid (PLGA) for PTT had been successfully constructed. And then they were swallowed by macrophages as cell-based biocarriers to target the tumor and promote the solid tumor ablation *in vivo* animal experiments. This system is expected to bring a huge application potential in visual-guided dual-modal therapeutic platform for tumor targeting therapy *in vivo*.

***Keywords:*** *Tumor-associated macrophage, immunotherapy, tungsten oxide ($W_{18}O_{49}$, WO)* nanoparticles*, near infrared (NIR) light, photothermal therapy (PTT)*

## 1. Introduction

Macrophages are highly versatile effector cells as essential components of immune system.[1-5] They can infiltrate into tumor microenvironment in high numbers for inhibiting tumor growth and killing tumor cells by phagocytosis.[6-10] Besides, they can also secrete a wide array of cytokines to activating the anti-tumor immune response, such as TNF α, IL β, etc.[11-13] Hence, drawn these performances, the macrophages can specifically kill tumor cells and carry therapeutic reagents targeting to the tumor region.[14-19] However, the service life of the macrophages is only about two weeks and then the performance of killing tumors will follow it loss. Furthermore, this cell-killing effectiveness is also limited, so it is necessary to combine it with another way of killer tumor cells, such as photothermal therapy (PTT) which has high treatment efficiency to target tumor cells while minimizing collateral injury to healthy tissue.[20-23] In photothermal therapy protocol, tungsten oxide ($W_{18}O_{49}$, WO) as its strong localized surface plasmon resonances can absorb 808 nm near infrared (NIR) light with higher efficiency to steadily and repeatedly convert it into local high heat. Compared with metal nanostructures of commonly used PTT candidates (e.g., Ge nanoparticles, Pd-based nanosheets and Au nanostructures), $W_{18}O_{49}$ NPs possess several advantages such as cheaper costs and higher yields, and thus serve as an excellent potential photothermal reagent for PTT *in vitro* and *in vivo*.[24-26] Nevertheless, the

WO cannot be used for imaging *in vivo* because of its lack of fluorescence properties. Hence, the applications of immunotherapy and photothermal therapy are seriously limited *in vivo* due to lack of imaging-guided performance.

In this paper, to track WO and macrophages, the indocyanine green (ICG) as a excellent water soluble near infrared fluorescence dye was used for imaging-guided combination therapy *in vivo*.[27-29] The WO and ICG assembled PLGA nanoparticles (WO+ICG)@PLGA had been developed for ICG imaging-guided oncotherapy. After that, the macrophages as cell-based biocarriers were used for better delivering the (WO+ICG)@PLGA nanoparticles to the tumor region. The (WO+ICG)@PLGA@macrophage (WIPM) delivery system consists of four parts: 1) The $W_{18}O_{49}$ with substantial absorption in the 808 nm near-infrared (NIR) light and effective photothermal response had been used for PTT; 2) Indocyanine green (ICG), a fluorescent dyes to help visualize the macrophage and WO *in vivo*, could be excited by 710 nm wavelengh light; 3) The polylactic-co-glycolic acid (PLGA) worked as a three dimension template for loading and preventing WO and ICG from aggregation and diffusion *in vivo*; 4) (WO+ICG)@PLGA was devoured by macrophages as a cell-based biocarrier to target the tumor microenvironment and promote the kill efficiency for tumor cells by activating anti-tumor immune response and photothermal therapy (PTT)

(as shown in Fig. 1). This novel immunotherapy and photothermal therapy system has a huge application potential in visual-guided dual-modal therapeutic platform for tumor targeting treatment *in vivo*.

## 2. Materials and methods

### 2.1 Materials

Indocyanine green (ICG), Tungsten(VI) chloride ($WCl_6$, ≥99.9%), 1-propyl alcohol (anhydrous, 99.7%), ethanol (ACS reagent, ≥99.5%), poly(lactic-co-glycolic) acid (PLGA), Poly(vinyl alcohol) (PVA, ≥99%), 1,2-dihexadecanoyl-sn-glycero-3-phosphoethanolamine, cholesterol (reagent grade, ≥92.5%) and FITC were all obtained from Sigma-Aldrich (USA).

### 2.2 Synthesis of WO and (WO+ICG)@PLGA nanoparticles

The $W_{18}O_{49}$ nanoparticles were synthesised according to previous reported with some improvement.[24] Typically, $WCl_6$ (0.5g) was dissolved in n-propyl alcohol by magnetically stirring. And then the above mixing solution was transferred into a reaction still to obtained the $W_{18}O_{49}$ (WO) nanorod-bundled nanostructures after maintaining at 200 °C for 10 h. $W_{18}O_{49}$ (WO) precipitate was grinded, ultrasonic processed and collected by centrifugation to obtain the $W_{18}O_{49}$ (WO) prills. Final precipitate was kept in dichloromethane after washed.

WO and PLGA co-assembling WO@PLGA and (WO+ICG)@PLGA nanoparticles were synthesis according to the following method.[30] Briefly, 0.5g PLGA was dissolved in 10ml dichloromethane. Then they were added to an aqueous stabilizer mixture containing PVA (6 mg), ICG (1mg) and WO (1mg) in 2 ml water under high-power ultrasound at output 200 W. And then the mix emulsion solution was added a larger amount of 50ml PVA water solution under high-power ultrasound. The mix solution was continued to stirring at room temperature to remove organic solvent under magnetically stirring for 24h. Finally, after purified by centrifugation at 6000 rmp to remove PVA, the (WO+ICG)@PLGA nanoparticles samples were kept in water.

### 2.3 Fluorescence imaging *in vitro* and *in vivo*

Fluorescence imaging of all samples was monitored after excitation with 710 nm light by Berthold NightOWL LB 983 Imaging System (BERTHOLD, Germany). *In vitro* fluorescence imaging was operated by putting the sample into 96-well plates. The *in vivo* imaging was operated by injection of samples through the local or caudal vein injection. The photothermal efficiency was tested as follows: Samples were added into cuvette and irradiated for 10 min simultaneously with 1.5 W/cm$^2$ laser (MDL-N-808 (Cnilaser, China)). Temperature variation was monitored by infrared thermal imaging camera (Fluke, USA). To explore the

photothermal treatment efficiency, medium was replaced by new medium contained different treatments. The cells were incubated within the medium containing different samples for 24 h and then medium was discarded and washed by PBS. Fresh medium was added and the plates were kept at 37 ℃ before and during laser irradiation. The cell viability was evaluated using MTT assay. The cytotoxicity of photothermal treatment was evaluated by Calcein-AM living cells stained assay according to the instructions (Invitrogen).[31-33]

Healthy female C57/B6 mice of 20–25 g body weight were purchased from HFK Technology Co., Ltd. (Beijing). Animal experiments were performed in accordance with the statutory requirements of People's Republic of China (GB14925-2010). To develop melanoma tumor model, $5\times10^4$ B16-F0 melanoma cells were injected subcutaneously (s.c.). The treatment was carried out when the tumor growth to 300 $mm^3$. The (WO+ICG)@PLGA loading macrophages in 100 ul PBS was injected into the tumor. The fluorescence imaging of mouse from ICG was monitored after excitation with 710 nm light by Berthold NightOWL LB 983 Imaging System (BERTHOLD, Germany).

### 2.4 *In vivo* antitumor assessment

Tumor size was monitored by vernier caliper, and tumor volume (V) was calculated as V=Length×Width×(Length+Width)/2. When tumor

volume reached about 300-350 $mm^3$, mice were randomly distributed into five groups: The control group 1 received PBS tail vein injection only, control group 2 was exposed to NIR laser of 1.5 $W/cm^2$ for 10 min, control group 3 received (WO+ICG)@PLGA nanoparticles (WIP) tail vein injection only, control group 4 received $10^6$ Raw 264.7 cells tail vein injection only, and experimental group received the 0.5 mg/ml (WO+ICG)@PLGA nanoparticles loaded macrophages (WIPM) tail vein injection by $10^6$ Raw 264.7 cells and was also exposed to 808 nm NIR laser light after injection for 72h .

Subsequently, tumor size and body weight of each mouse were recorded everyday. At days 15, some mice were sacrificed and tumors were collected. Then photos of tumors were taken by a digital camera (Nikon, Japan). After that, tumors were washed with saline three times and fixed in 10% neutral-buffered formalin. For the hematoxylin and eosin (H&E) and TUNEL assay ((Roche, Switzerland), paraffin tumor sections were stained and observed by an Fluorescence Inversion Microscope System (Olympus, Japan).[33, 34]

**2.5 Statistical analyses**

Data were expressed as mean ± standard deviation (SD) of experiments and each experiment group contained 5 repeated samples. Data analysis was performed using OriginPro 8.0 and Microsoft Excel. The

significance between groups were analyzed using unpaired two-tailed t-test (compared two groups) and one-way analysis of variance (ANOVA) (compared multiple groups) by Statistics Analysis System (* $p < 0.05$ and ** $p < 0.01$, respectively). $p < 0.05$ was considered as significant.[34]

# 3 Results and discussion

## 3.1 The Synthetic Process and Physicochemical Characterization of (WO+ICG)@PLGA

Preparation process of (WO+ICG)@PLGA could be divided into four steps (as shown in Fig. 2A and Fig. S1). Firstly, the $W_{18}O_{49}$ (WO) nanorod-bundled nanostructures were synthesized by solvothermal method with $WCl_6$ after 200°C reaction for 10 h. Secondly, the small particle size of $W_{18}O_{49}$ (WO) nanoparticles were obtained after grinding, processing with ultrasonic and centrifugal purification from the preparation nanorod-bundled nanostructures. Finally, the (WO+ICG)@PLGA nanoparticles were obtained by ultrasonic emulsification of WO, indocyanine green (ICG) and polylactic-co-glycolic acid (PLGA) and centrifugal purification. Such ICG and WO co-assembling PLGA nanoparticles ((WO+ICG)@PLGA) integrated the unique optical properties of fluorescence imaging and photothermal therapy.

The physical and chemical properties of as-obtained (WO+ICG)@PLGA were examined by transmission electron microscope (TEM), X-ray diffraction (XRD) and energy-dispersive X-ray spectroscopy (EDX). The Fig. 2B and Fig. S2 presented special TEM imaging of $W_{18}O_{49}$ nanorod-bundled nanostructures obtained after reaction for 10 h, which were densely packed together to form the bundles (Fig. 2B1). The WO nanorod-bundled nanostructures were spindle-shape (length within 500-700 nm, width about 200 nm) and with some spine and obvious embossment, and then it was difficult that were applied to *in vivo* experiment. Hence, it was necessary for processing the WO nanorod-bundled nanostructures. As shown in Fig. 2B2, the WO@PLGA nanoparticles were all some spherical particles and had good monodispersity with an average diameter of 200 nm and very clear profile after grinding and ultrasonic emulsification with polylactic-co-glycolic acid (PLGA). The (WO+ICG)@PLGA nanoparticles were prepared using the same method and the appearance characteristics was without any change with WO@PLGA in Fig. 2B3. The pure phase of WO@PLGA nanoparticles were identified by XRD spectrum and compared with standard data for $W_{18}O_{49}$ (JCPDS 71–2450)[24] (Fig. 2C). The chemical element was analyzed by energy-dispersive X-ray spectroscopy (EDX) (Fig. 2D). These results suggested that the (WO+ICG)@PLGA was successful obtained.

The optical property of as-obtained these samples were studied using UV-VIS spectrophotometers (UV-2450, Shimadzu). The UV–Vis spectrum of (WO+ICG)@PLGA displayed an extended absorption band near 600-850 nm due to the loading of ICG (Fig. 2E). As depicted in inset of Fig. 2E, aqueous solution of WO@PLGA presented blue color and (WO+ICG)@PLGA presented bottle green color due to the loading of ICG. These important features of (WO+ICG)@PLGA demonstrated that the ICG was successfully loading into the PLGA nanoparticles. In order to evaluate the imaging effect of (WO+ICG)@PLGA, the aqueous solution of different samples were added into the 96-well plate. The fluorescence intensity from various samples was monitored by *in vivo* imaging system As shown in Fig. 2F, the WO@PLGA line did not show any fluorescence, while the vertical columns of free ICG and (WO+ICG)@PLGA had intense fluorescence. With the increase of samples concentration, the fluorescence intensity enhanced. The results indicated that (WO+ICG)@PLGA could be well used for fluorescence imaging. In addition, in order to clearly see ICG position in (WO+ICG)@PLGA nanoparticles, the fluorescence microscope photos were provided, and in the pictures, the oil phase shell structure was composed by FITC with the PLGA and the ICG was aqueous phase in core (Fig. 2G).

### 3.2 The biocompatibility of WO@PLGA and (WO+ICG)@PLGA nanoparticles

To investigate the biocompatibility of nanoparticles, standard methyl thiazolyl tetrazolium (MTT) assay was performed to detect the viabilities of Raw 264.7 cells (a source of the rat macrophages). Cells were incubated with different concentrations of samples in 37℃ for 24 h, and the results showed that no significant cell death was detected when treated with WO@PLGA and (WO+ICG)@PLGA. Although with increase of the concentration cell viability decreased in all these samples, at a high concentration of 1mg/ml the cell viability was more than 80% (Fig. 3B). The green fluorescent dye, Calcein-AM, was used to label living cells. As seen in Fig. 3A, all cells incubated with WO@PLGA and (WO+ICG)@PLGA nanoparticles were labeled with strong green fluorescence, manifesting cells were alive. Meanwhile, these results were also confirmed by flow cytometry studies (Fig. 3C1 and C2), and the similar results were also verified by B16 cells and hemolytic test (Fig. S3 and S4). These results illustrated that the WO@PLGA and (WO+ICG)@PLGA nanoparticles had good biocompatibility.

### 3.3 The phagocytosis test of macrophages for (WO+ICG)@PLGA nanoparticles

Phagocytosis is an important characteristic of macrophages. In order to test whether macrophages had strong phagocytosis function, the Raw 264.7 cells were incubated with different concentrations (WO+ICG)@PLGA nanoparticles. The fluorescence intensity of ICG was getting higher, with the concentrations increase of (WO+ICG)@PLGA nanoparticles after incubating 2 h. Almost all the cells were filled with the ICG, when the concentration of (WO+ICG)@PLGA nanoparticle arrived at 0.5 mg/ml. Meanwhile, the results were also confirmed by flow cytometry studies (Fig. S5).

In order to test whether macrophages still had phagocytosis function after uptaking the (WO+ICG)@PLGA nanoparticles, phagocytosis experiment was designed. Firstly, the Raw 264.7 cells were incubated with (WO+ICG)@PLGA nanoparticles. Afterwards, the B16 tumor cells were labeled with FITC-phalloidin (Green fluorescent probe) in Fig. 4A1. Finally, the Raw 264.7 cells of loading (WO+ICG)@PLGA nanoparticles were incubated with the green B16 cells. As seen in Fig. 4, after macrophages incubated with (WO+ICG)@PLGA nanoparticles, the strong red fluorescence was observed in Raw 264.7 cells, which indicated that the (WO+ICG)@PLGA nanoparticles had already been uptaked into macrophages (Fig. 4A2). Then they were incubated with FITC-phalloidin labeled B16 cells for 6 h. After the culture medium was replaced, the green fluorescence was found in the macrophages (Fig. 4A3), which

suggested that the B16 cell debris was swallowed into macrophages and laser confocal fluorescence microscopy was also used for observing the phagocytosis (Fig. 4B). Meanwhile, the results were also confirmed by flow cytometry studies. All these results suggested that the macrophages still had phagocytosis function for tumor cells after the (WO+ICG)@PLGA uptake. And macrophages as the therapeutic reagent could be also used to kill tumor cells by its phagocytosis.

### 3.4 The photothermal performance of (WO+ICG)@PLGA nanoparticles

Various samples were added into different quartz colorimetric utensil, and with 1.5 W/cm$^2$ 808 nm NIR laser irradiating these samples for 10 min, temperature changes of each group were monitored using thermometer and thermal imaging camera. Negligible temperature increase was monitored in PLGA group. But WO@PLGA and (WO+ICG)@PLGA groups could produce remarkable bulk heat and the temperature was more than 50℃under the same condition（Fig. 5A and B）. As shown in Fig. 5A, after multiple exposures for 808 nm NIR laser, WO as a transition metal oxides still could produce stable hyperthermia, while conventional organic reagents were often used only once under NIR laser. This phenomenon illustrated that the WO@PLGA and (WO+ICG)@PLGA nanoparticles could become an excellent photothermal reagent for PTT.[24-26] Meanwhile, the damage effect of

photothermal therapy in B16 cells was tested. As shown in Fig. S6 and S7, most of the cancer cells had been killed by irradiating with 808 nm NIR laser for 10 min after incubation with (WO+ICG)@PLGA nanoparticles. These results demonstrated that the (WO+ICG)@PLGA nanoparticles had the heat generation capacity under NIR light exposure, and it could be used for photothermal therapy (PTT).

In order to prove the (WO+ICG)@PLGA nanoparticles could be used for fluorescence imaging and PTT during tumor treatment *in vivo*, we carried out a series of experiment to investigate the fluorescence imaging and photothermal effects of various samples in the B16 subcutaneous tumor model in C57/B6 mice by intratumor injection. As shown in Fig. 5C, there was not any fluorescence in PLGA group under *in vivo* imaging and there was also no obvious difference in temperature change under irradiation of NIR laser light for 10 min. However, temperature was remarkablely increased for WO@PLGA and (WO+ICG)@PLGA groups under the same condition. Nonetheless, only the (WO+ICG)@PLGA group had intense fluorescence under *in vivo* imaging. It illustrated that the WO@PLGA and (WO+ICG)@PLGA nanoparticles indeed could cause photo-heat conversion efficiently *in vivo* under 808 nm NIR laser irradiating. At the same time, these results indicated that only (WO+ICG)@PLGA nanoparticles could be simultaneously used for fluorescence imaging and photothermal therapy, which they could be

used as hyperthermia reagents for imaging-guided tumor PTT *in vivo*.

### 3.5 *In vivo* suppression of tumor in mice using (WO+ICG)@PLGA nanoparticles loaded macrophages

To test the targeting effect of (WO+ICG)@PLGA nanoparticles loaded macrophages (WIPM) *in vivo*, the samples were injected into the B16 subcutaneous tumor model in C57/B6 mice by caudal vein. The treatment was carried out when the tumor volume grew to 300 $mm^3$. The plentiful (WO+ICG)@PLGA nanoparticles loaded macrophages (WIPM) gathered to the tumor area after intravenous injection for 24 h (Fig. 6A), consistent with the results reported in many literatures.[13-15, 35] After euthanasia, the main internal organs and tumor from the mice different treatment groups mice were taken out, and the fluorescence intensity was detected by *in vivo* imaging system. As shown in Fig. 6B and S8, the excised tumor had a very higher fluorescence intensity for (WO+ICG)@PLGA nanoparticles loaded macrophages group compared with free ICG and (WO+ICG)@PLGA alone groups. The phenomenon illustrated that (WO+ICG)@PLGA nanoparticles loaded macrophages could be used for targeting the tumor region and fluorescence imaging to visual tumor treatment *in vivo*. Meanwhile, there was a very good heat production effect *in vivo* after irradiated by 808 nm NIR laser light for (WO+ICG)@PLGA nanoparticles loaded macrophages group (Fig. 6C

and S9-S12). These results suggested that macrophages help to significantly improve (WO+ICG)@PLGA nanoparticles tumor-targeting delivery ability and photo-thermal conversion efficiency *in vivo*.

In order to verify that macrophages could produce anti-tumor cytokines *in vivo*, there were five groups of experiment were designed. The group 1 received PBS tail vein injection only, group 2 exposed to NIR laser of 1.5 W/cm$^2$ for 10 min, group 3 received (WO+ICG)@PLGA nanoparticles (WIP) tail vein injection only, group 4 received $10^6$ Raw 264.7 cells tail vein injection only, and group 5 received the 0.5 mg/ml (WO+ICG)@PLGA nanoparticles loaded macrophages tail vein injection by $10^6$ Raw 264.7 cells. After treatment different time, the anti-tumor cytokines in mice blood were detected using the ELISA method. The level of TNF α and IL β, which they were widely used for anti-tumor immunotherapy,[11-13] had a significant increase for macrophages group and (WO+ICG)@PLGA nanoparticles loaded macrophages group (Fig. 6D and E). These results showed that macrophages loading (WO+ICG)@PLGA nanoparticles still could be used in immunotherapy for anti-tumor *in vivo*.

The group 1 received PBS tail vein injection only, group 2 exposed to NIR laser of 1.5 W/cm$^2$ for 10 min, group 3 received (WO+ICG)@PLGA nanoparticles (WIP) tail vein injection only, group 4 received $10^6$ Raw

264.7 cells tail vein injection only, and group 5 received the 0.5 mg/ml (WO+ICG)@PLGA nanoparticles loaded macrophages tail vein injection by $10^6$ Raw 264.7 cells and exposed to 808 nm NIR laser light.

As a proof-of-concept study, oncotherapy effect *in vivo* was further evaluated. There were four groups of experiment were designed. The control group 1 received PBS tail vein injection only, control group 2 exposed to NIR laser of 1.5 W/cm$^2$ for 10 min, control group 3 received (WO+ICG)@PLGA nanoparticles (WIP) tail vein injection only and experimental group received the 0.5 mg/ml (WO+ICG)@PLGA nanoparticles loaded macrophages tail vein injection by $10^6$ Raw 264.7 cells and exposed to 808 nm NIR laser light after injection for 72 h. After 15 days of treatment in different ways, the digital photos of excised tumors from each group mouse displayed that the tumor size of the experimental group was the smallest (Fig. 6F and S13). Besides, the volume of each group tumors were measured everyday during different treatment. Compared with the tumor volumes of control group 1-3, it was obviously suppressed in 300 mm$^3$ for experimental group after 15 days treatment and the experiment group showed slower tumor growth (Fig. 6G). In addition, the tumor weight of the experiment group was measured too, and compared with the weight about 1.4 g in control groups 1-3, it was only 0.15 g for experimental group after 15 days treatment (Fig. 6H). These results proved the commendable anti-tumor ability of the

(WO+ICG)@PLGA nanoparticles loaded macrophages under irradiation 808 nm NIR laser light. What's more, the survival time of mice was also observed, and the result showed that there was a significant longer survival period in experimental group (Fig. 6I and Fig. S14). And these results indicated that under the targeting of macrophages, the combination therapy of immunotherapy and photothermal therapy using (WO+ICG)@PLGA nanoparticles, which they made the tumor acquire adequate temperature to be destructed under NIR laser exposure, could clearly restrain growth tumor. Treated with PBS, laser or (WO+ICG)@PLGA nanoparticles alone, however, were insufficient to achieve tumor destruction.

Furthermore, the B16 xenograft tumors were collected and the histological analyses were also performed using TUNEL staining. More significant tumor necrosis with severe structural damage could be observed in group 4, compared with another three groups (Fig. 7A and B). These results certified the excellent anti-tumor ability of group 4 which received the 0.5 mg/ml (WO+ICG)@PLGA nanoparticles loaded macrophages tail vein injection by $10^6$ Raw 264.7 cells and exposed to 808 nm NIR laser light. During the animal experiments, weights of these tumor-bearing mice and histological analyses of main organs indicated no obvious difference in the four groups for suggesting excellently biocompatibility for the visual-guided dual-modal therapeutic platform *in*

*vivo* (Fig. 7C and Fig. S15). All these results illustrated that (WO+ICG)@PLGA nanoparticles loaded macrophages synergistic therapeutic system could successfully inhibit the growth of tumor *in vivo* with the help of immunotherapy and photothermal therapy.

## 4. Conclusions

In summary, we had successfully constructed the fluorescence image-guided photothermal therapy reagents based on (WO+ICG)@PLGA) nanoparticles. In our design, to improve their tumor targeting, the macrophages as cell-based biocarriers were employed for delivery the (WO+ICG)@PLGA nanoparticles. The macrophages carried these nanoparticles still had phagocytosis to tumor cells and could also secret plenty of anti-tumor cytokines for immunotherapy of carcinoma. We also further elucidated the superior solid tumor suppression efficiency of the (WO+ICG)@PLGA nanoparticles loaded macrophages targeting biocarriers delivery system *in vivo*. The system achieved a significant antitumor effect by activating immunotherapy and photothermal therapy *in vivo*. Hence, such kind of (WO+ICG)@PLGA nanoparticles loaded macrophages delivery system has great potential applications as targeting biocarriers loading drugs and imaging agents for visual-guided synergistic therapy *in vivo*.

## Conflicts of interest

There are no conflicts to declare.

## Acknowledgements

This work was sponsored by National Key Research and Development Program of China (2017YFA0205104), National Natural Science Foundation of China (51373117, 51573128 and 81771970), Tianjin Natural Science Foundation (15JCQNJC03100).

## References


1. L. Bingle, N. J. Brown and C. E. Lewis, *J. Pathol.,* 2002, **196**, 254-265.
2. A. Varin and S. Gordon, *Immunobiology*, 2009, **214**, 630.
3. D. M. Pardoll, *Nat. Rev. Cancer*, 2012, **12**, 252-264.
4. A. Mantovani and A. Sica, *Curr. Opin. in Immunol.*, 2010, **22**, 231.
5. D. G. DeNardo, J. B. Barreto, P. Andreu, L. Vasquez, D. Tawfik, N. Kolhatkar and L. M. Coussens, *Cancer Cell*, 2009, **16**, 91-102.
6. P. Allavena, A. Sica, G. Solinas, C. Porta and A. Mantovani, *Crit. Rev. Oncol. Hemat.,* 2008, **66**, 1.
7. T. Chanmee, P. Ontong, K. Konno and N. Itano, *Cancers*, 2014, **6**, 1670.
8. N. B. Hao, M. H. Lü and Y. H. Fan, *Clin. Dev. Immunol.*, 2012, **2012**, 948098.
9. P. F. Slivka, C. L. Dearth, T. J. Keane, F. W. Meng, C. J. Medberry, R. T. Riggio, J. E. Reing and S. F. Badylak, *Biomater. Sci.*, 2014, **2**, 1521.
10. C. Wu, H. Chen, X. Wu, X. Cong, L. Wang, Y. Wang, Y. Yang, W. Li and T. Sun, *Biomater. Sci.*, 2017, **5**, 153.
11. A. Mantovani, T. Schioppa, C. Porta, P. Allavena and A. Sica, *Cancer. Metast. Rev.,* 2006, **25**, 315-322.

12. A. Sica, T. Schioppa, A. Mantovani and P. Allavena, *Eur. J. Cancer,* 2006, **42**, 717.

13. Y. Luo, H. Zhou, J. Krueger, C. Kaplan, S. H. Lee, C. Dolman, D. Markowitz, W. Wu, C. Liu and R. A. Reisfeld, *J. Clin. Invest.,* 2006, **116**, 2132.

14. G. Germano, R. Frapolli, C. Belgiovine, A. Anselmo, S. Pesce, M. Liguori, E. Erba, S. Uboldi, M. Zucchetti and F. Pasqualini, *Cancer Cell*, 2013, **23**, 249.

15. R. Z. Panni, D. C. Linehan and D. G. DeNardo, *Immunotherapy*, 2013, **5**, 1075-1087.

16. F. Chellat, Y. Merhi, A. Moreau and L. H. Yahia, *Biomaterials*, 2005, **26**, 7260-7275.

17. L. Yan, Y. Gao, R. Pierce, L. Dai, J. Kim and M. Zhang, *Mater. Res. Express,* 2014, **1**, 025007.

18. E. M. Dijkgraaf, M. Heusinkveld, B. Tummers, L. T. Vogelpoel, R. Goedemans, V. Jha, J. W. Nortier, M. J. Welters, J. R. Kroep and V. D. B. Sh, *Cancer Research*, 2013, **73**, 2480-2492.

19. H. Hirschberg and S. J. Madsen, *J Neuroimmune Pharmacol*, 2017, **12**, 99.

20. H. Zhu, P. Cheng, P. Chen and K. Pu, *Biomater. Sci.*, 2018.

21. R. Chen, X. Zheng, H. Qian, X. Wang, J. Wang and X. Jiang, *Biomater. Sci.*, 2013, **1**, 285-293.

22. Y. Peng, J. Nie, W. Cheng, G. Liu, D. Zhu, L. Zhang, C. Liang, L. Mei, L. Huang and X. Zeng, *Biomater. Sci.*, 2018.

23. H. Chen, X. Chi, B. Li, M. Zhang, Y. Ma, S. Achilefu and Y. Gu, *Biomater. Sci.*, 2014, **2**, 996-1006.

24. K. Deng, Z. Hou, X. Deng, P. Yang, C. Li and J. Lin, *Adv. Funct. Mater.*, 2016, **25**, 7280-7290.

25. Z. Chen, Q. Wang, H. Wang, L. Zhang, G. Song, L. Song, J. Hu, H. Wang, J. Liu and M. Zhu, *Adv. Mater.*, 2013, **25**, 2095-2100.

26. B. Zheng, J. Wang, H. Pan, H. Chen, W. Ji, Z. Liao, X. Gong, H. Wang and C. Jin, *J. Colloid Interf. Sci.*, 2017, **506**, 460.

27. C. Zheng, M. Zheng, P. Gong, D. Jia, P. Zhang, B. Shi, Z. Sheng, Y. Ma and L. Cai, *Biomaterials*, 2012, **33**, 5603-5609.

28. X. Zheng, D. Xing, F. Zhou, B. Wu and W. R. Chen, *Mol. Pharmaceut.,* 2011, **8**, 447.

29. Y. Ma, S. Tong, G. Bao, C. Gao and Z. Dai, *Biomaterials*, 2013, **34**, 7706-7714.

30. H. Wang, P. Zhao, W. Su, S. Wang, Z. Liao, R. Niu and J. Chang, *Biomaterials*, 2010, **31**, 8741-8748.

31. B. Zheng, X. Gong, H. Wang, S. Wang, H. Wang, W. Li, J. Tan and J. Chang, *Nanotechnology*, 2015, **26**, 425102.

32. B. Zheng, L. Su, H. Pan, B. Hou, Y. Zhang, F. Zhou, X. Wu, X. Gong, H. Wang and J. Chang, *Adv. Mater.*, 2016, **28**, 707.

33. B. Zheng, H. B. Chen, P. Q. Zhao, H. Z. Pan, X. L. Wu, X. Q. Gong, H. J. Wang and J. Chang, *ACS Appl. Mater. Interfaces,* 2016, **8**, 21603.

34. B. Zheng, H. Wang, H. Pan, C. Liang, W. Ji, L. Zhao, H. Chen, X. Gong, X. Wu and J. Chang, *Acs Nano*, 2017.

35. T. Maldiney, A. Bessière, J. Seguin, E. Teston, S. K. Sharma, B. Viana, A. J. Bos, P. Dorenbos, M. Bessodes and D. Gourier, *Nat. Mater.*, 2014, **13**, 418.

# Figures:

Fig. 1. Schematic plot indicated applications of (WO+ICG)@PLGA loading macrophages to target the tumor region and ICG fluorescence imaging-guided visual immunotherapy and photothermal therapy *in vivo*. Thereinto, ICG and WO assembled PLGA nanoparticles ((WO+ICG)@PLGA) had been used for ICG imaging-guided oncotherapy. The macrophages as cell-based carriers were employed for carrying the (WO+ICG)@PLGA nanoparticles to target the tumor region and activate the anti-tumor immune response by phagocytosis and secreting TNF α and IL β. The (WO+ICG)@PLGA@macrophage (WIPM) delivery system consists of four parts: 1) The $W_{18}O_{49}$ with substantial absorption in the near-infrared (NIR) light and efficient photothermal response had been used for photothermal therapy; 2) Indocyanine green (ICG), a fluorescent dye to help visualize the combined therapeutic system *in vivo*, could be excited by 710 nm light; 3) The polylactic-co-glycolic acid (PLGA) worked as a three dimension template for loading and preventing WO and ICG from aggregation and diffusion *in vivo*; 4) (WO+ICG)@PLGA was devoured by macrophages as a biocarrier to target the tumor microenvironment and promote the kill efficiency for tumor cells by activating anti-tumor immune response and photothermal therapy *in vivo*.

Fig. 2. (A) Schematic plot of preparation of (WO+ICG)@PLGA; TEM picture of (B1) $W_{18}O_{49}$, (B2) WO@PLGA, (B3) (WO+ICG)@PLGA nanoparticles; (C) The X-ray powder diffraction pattern of as-obtained

WO@PLGA nanoparticles and the numerical value from standard data for $W_{18}O_{49}$ (JCPDS 71–2450).[24] (D) The EDX test for element analysis of WO@PLGA nanoparticles. (E) UV-Vis absorption spectrum for WO@PLGA, free ICG and (WO+ICG)@PLGA. The inserts showed macrophotograph of these samples. (F) Aqueous solutions of WO@PLGA, free ICG and (WO+ICG)@PLGA were respectively added into the 96-well plate according to various concentrations and the fluorescence intensity of them were monitored by *in vivo* imaging system. (G) ICG position in (WO+ICG)@PLGA particles by observing fluorescence microscope. The scale bars were 10 μm.

Fig. 3. The biocompatibility of the WO@PLGA and (WO+ICG)@PLGA nanoparticles. (A) The green fluorescent dye, calcein-AM, was used to label the live cells by Raw 264.7 cells and the results were visualized by fluorescence microscope. The cells incubated with WO@PLGA and (WO+ICG)@PLGA nanoparticles. The scale bars were 100 μm. (B) The MTT assay of WO@PLGA and (WO+ICG)@PLGA nanoparticles. The results of calcein-AM staining was quantified for (C1) WO@PLGA and (C2) (WO+ICG)@PLGA nanoparticles by flow cytometry (FCM).

Fig. 4. Macrophages phagocytosis activity test of (WO+ICG)@PLGA nanoparticles and tumor cells. (A1) The plasma membrane of B16 cells

was stained by FITC-Phalloidin ((Green fluorescent probe); (A2) The Raw 264.7 cells uptaken the (WO+ICG)@PLGA nanoparticles and DAPI; (A3) The Raw 264.7 cells after uptaking the (WO+ICG)@PLGA nanoparticles were gently digested and added into the green B16 cells. The scale bars were 100 μm. Each process cells of stained FITC and ICG were quantified with flow cytometry (FCM). (B) High-resolution laser confocal fluorescence microscopy was used for observing the phagocytosis of A3. The scale bars were 10 μm.

Fig. 5. The (WO+ICG)@PLGA nanoparticles could be used for fluorescence imaging and photothermal therapy (PTT). (A) The temperature repeated changes of PLGA, WO@PLGA and (WO+ICG)@PLGA were monitored within NIR laser irradiation every 10 minutes using thermometer. (B) The PLGA, WO@PLGA and (WO+ICG)@PLGA were added into different quartz colorimetric utensil with 1.5 W/cm$^2$ 808 nm NIR laser to irradiate for 10 min and temperature variations were detected by thermal imaging camera. (C) ICG imaging and photothermal photographs of PLGA, WO@PLGA and (WO+ICG)@PLGA in the C57/B6 mice within NIR laser irradiation for 10 min using *in vivo* imaging system and thermal imaging camera.

Fig. 6. *In vivo* imaging and combination therapy of tumor in C57/B6. (A)

Free ICG, (WO+ICG)@PLGA nanoparticles (WIP) and (WO+ICG)@PLGA nanoparticles loaded macrophages (WIPM) were injected into the B16 tumor-bearing mice model by caudal vein and *in vivo* imaging was used for detecting the fluorescence at 24 h. (B) The fluorescence intensity of excised tumor in B16 tumor-bearing mice after tail vein injection different samples including free ICG, (WO+ICG)@PLGA nanoparticles (WIP) and (WO+ICG)@PLGA nanoparticles loaded macrophages (WIPM). (C) B16 tumor-bearing mice treated by the (WO+ICG)@PLGA nanoparticles loaded macrophages using tail vein injection and then exposed to 808 nm NIR laser light. (D) Anti-tumor immune response after macrophages treatment. The level of TNF α in mice blood was detected by the ELISA after treatment different time. (E) The level of IL β in mice blood was detected by the ELISA after treatment different time. (F) Tumor size for treating with different treatments after 15 days. (G) Changes in tumor volumes for treating with different treatments within 15 days (n=5). (H) Tumor weight for treating with different treatments after 15 days (n=5). (I) Survival curve of B16 tumor-bearing mice with different treatments (n=5). Data represent mean ± SD; *P<0.05 and **P<0.01(one-way ANOVA).

Fig. 7. H&E and TUNEL staining of B16 xenograft tumors and examined the acute toxicity of different samples for the mice. (A) The H&E staining for the tumor after treating with different treatments 15 days. (B) The TUNEL staining for the tumor after treating with different treatments 15 days. (C) The H&E staining for the main internal organs after treating with different treatments 15 days. The scale bars were 100 μm.

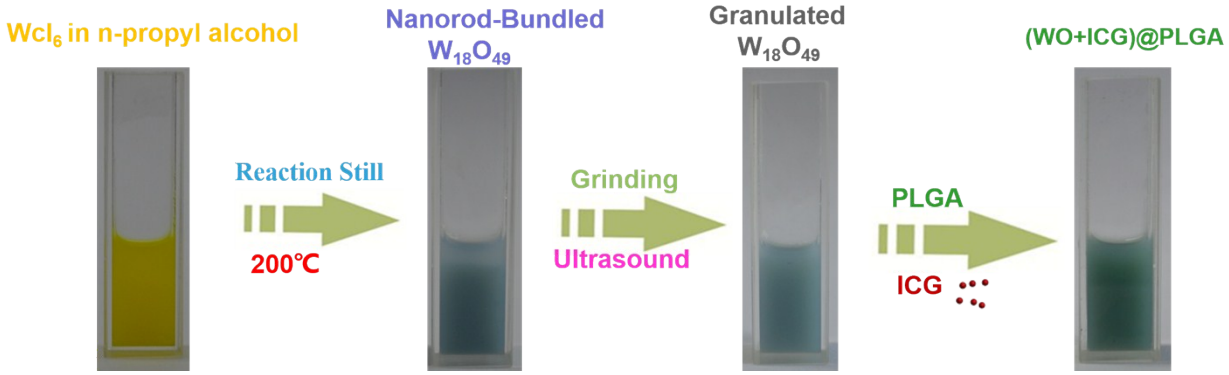


Fig. S1: The different state in the process of synthesis of (WO+ICG)@PLGA nanoparticles.

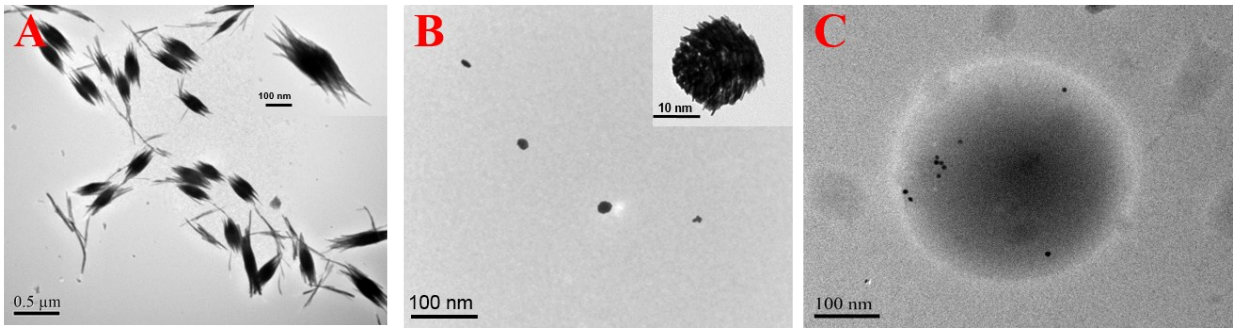


Fig. S2: The TEM images of (A) Nanorod-Bundled WO, (B) Granulated WO and (C) (WO+ICG)@PLGA nanoparticles.

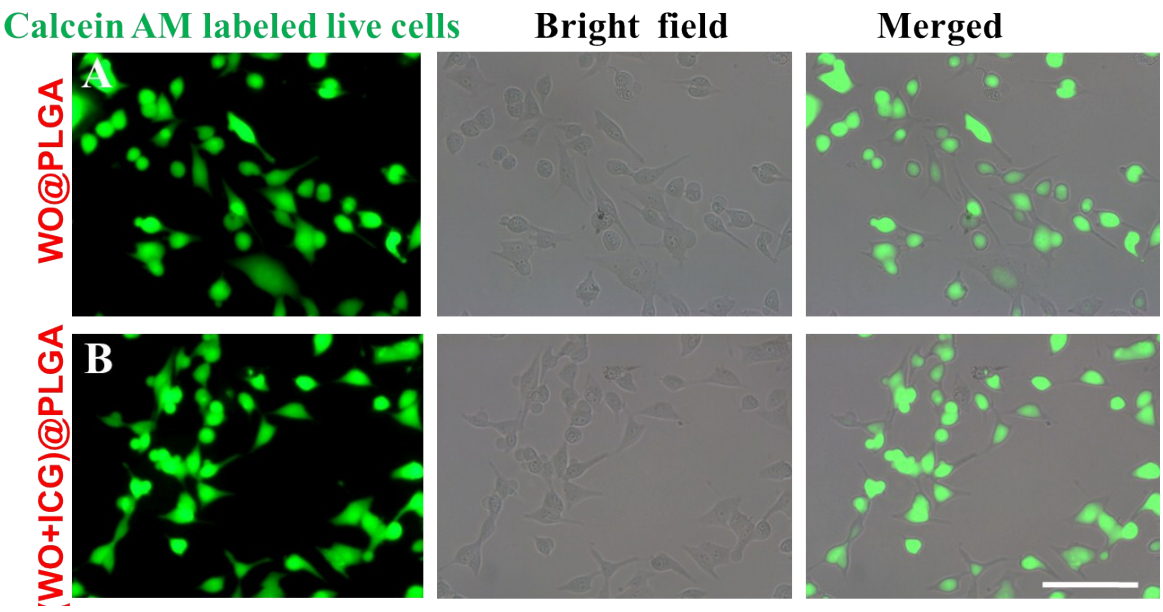


Fig. S3: The biocompatibility of the WO@PLGA and (WO+ICG)@PLGA nanoparticles in B16 cells. The green fluorescent dye, calcein-AM, was used to label the live cells by B16 cells and the results were visualized by fluorescence microscope. The cells incubated with WO@PLGA and (WO+ICG)@PLGA nanoparticles. The scale bars were 50 μm.

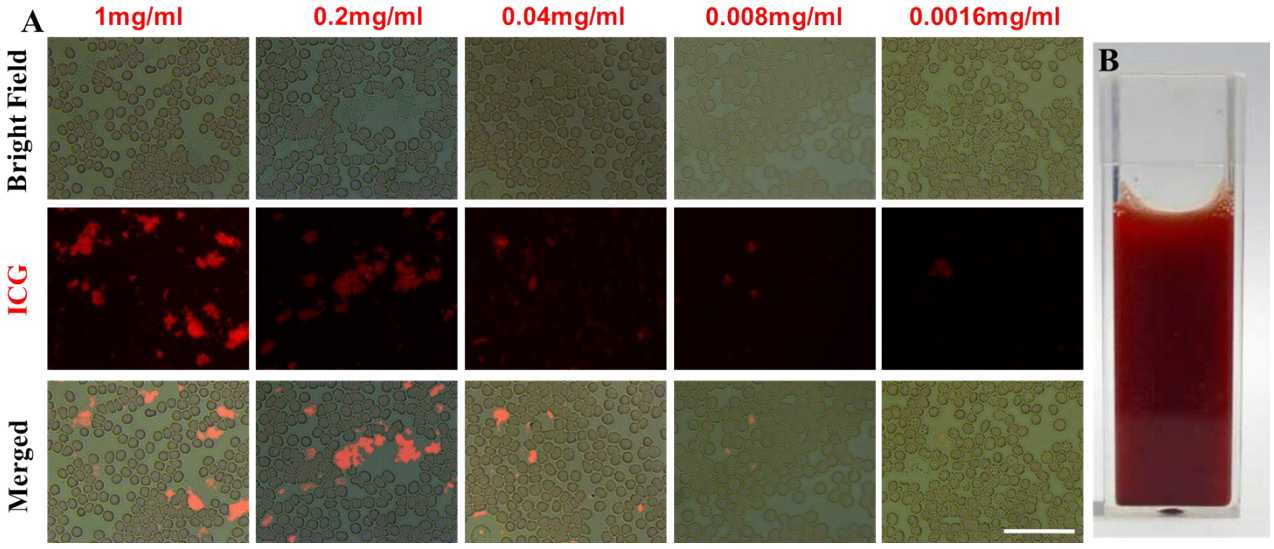


Fig. S4: The hemolytic test of various concentrations for (WO+ICG)@PLGA nanoparticles observe by (A) fluorescence microscope and (B) naked eye in cuvette. The scale bars were 100 μm.

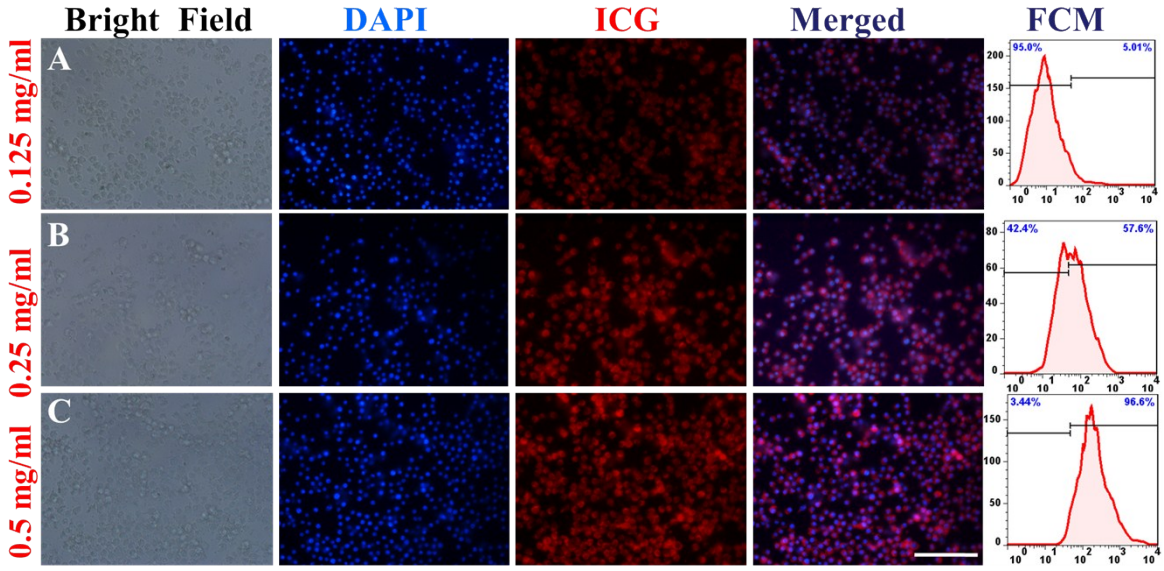


Fig. S5: The Phagocytosis efficiency of macrophage for (WO+ICG)@PLGA nanoparticles. The uptake of the (A) 0.125 mg/ml (WO+ICG)@PLGA nanoparticles, (B) 0.25 mg/ml (WO+ICG)@PLGA and (B) 0.5 mg/ml (WO+ICG)@PLGA nanoparticles for Raw 264.7 cells were visualized by fluorescence microscope. The scale bars were 100 μm. The cells stained ICG were quantified with flow cytometry (FCM) for 10, 000 cells.

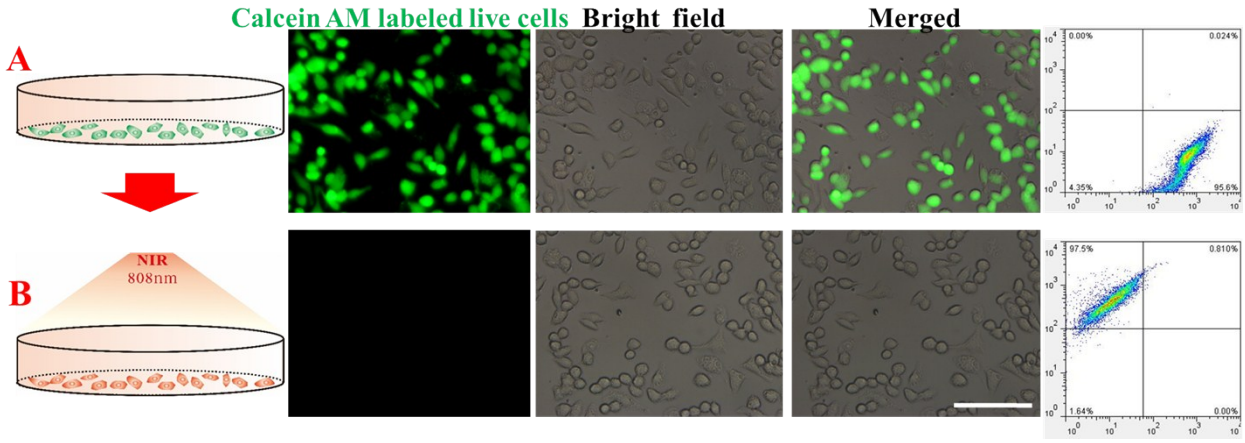


Fig. S6: The damage effect of photothermal therapy in B16 cells. (A) After incubation B16 cells with (WO+ICG)@PLGA nanoparticles, the B16 cells were labeled using calcein-AM. (B) The B16 cells were irradiated with 808 nm NIR laser for 10 min after incubation with (WO+ICG)@PLGA nanoparticles. The scale bars were 100 μm. The results of calcein-AM staining was quantified with flow cytometry (FCM) for 10, 000 cells.

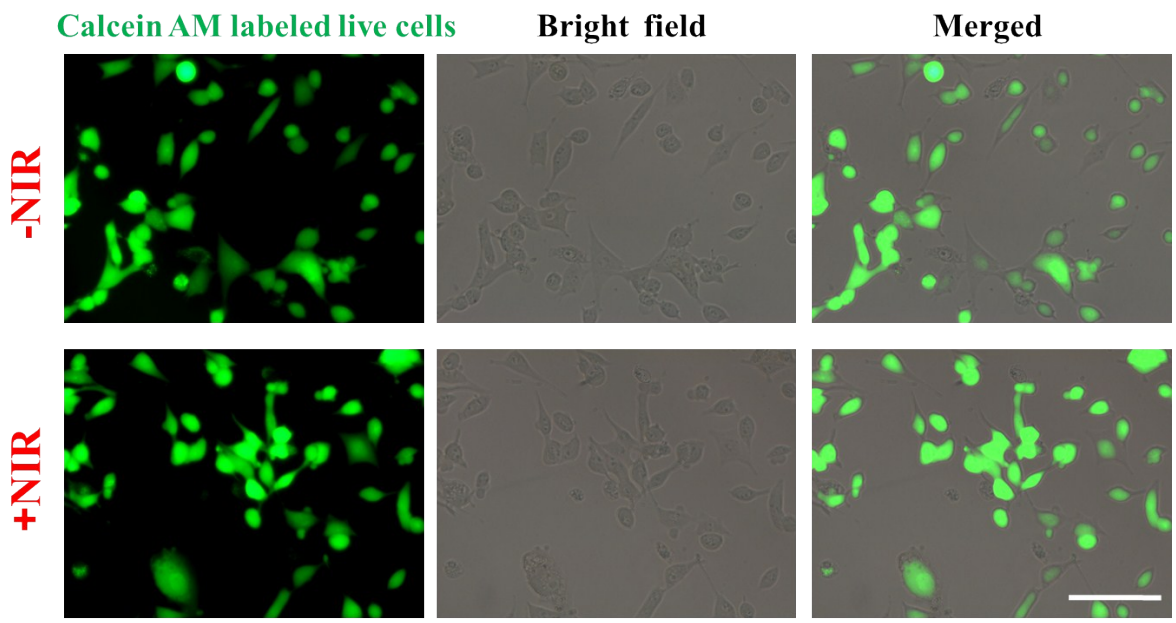


Fig. S7: The biocompatibility of the 808 nm near infrared light (NIR) exposure for 10 min in B16 cells without incubation of (WO+ICG)@PLGA. The green fluorescent dye, calcein-AM, was used to label the live cells by B16 cells and the results were visualized by fluorescence microscope. The scale bars were 100 μm.

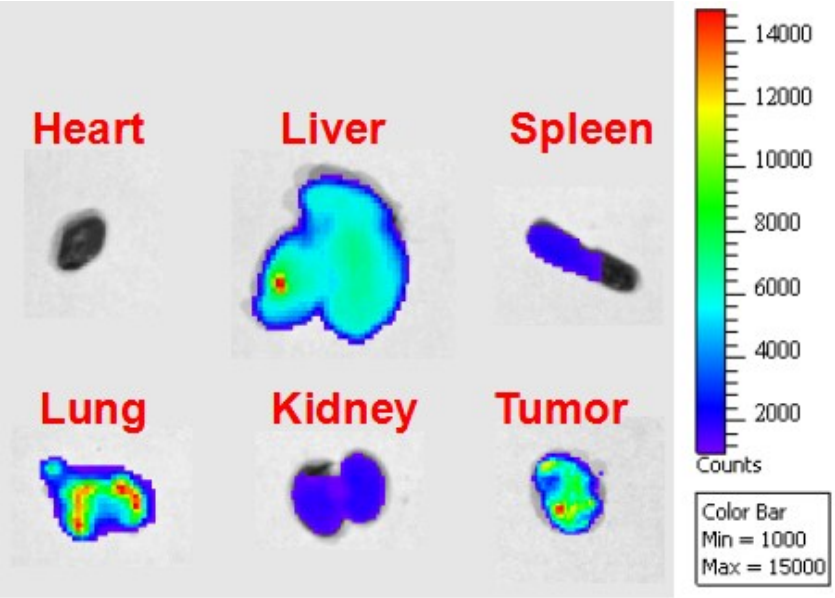


Fig. S8: The main internal organs and tumor of mice after (WO+ICG)@PLGA nanoparticles loaded macrophages using tail vein injection for 24 h were taken out, and the fluorescence intensity were detected by *in vivo* imaging.

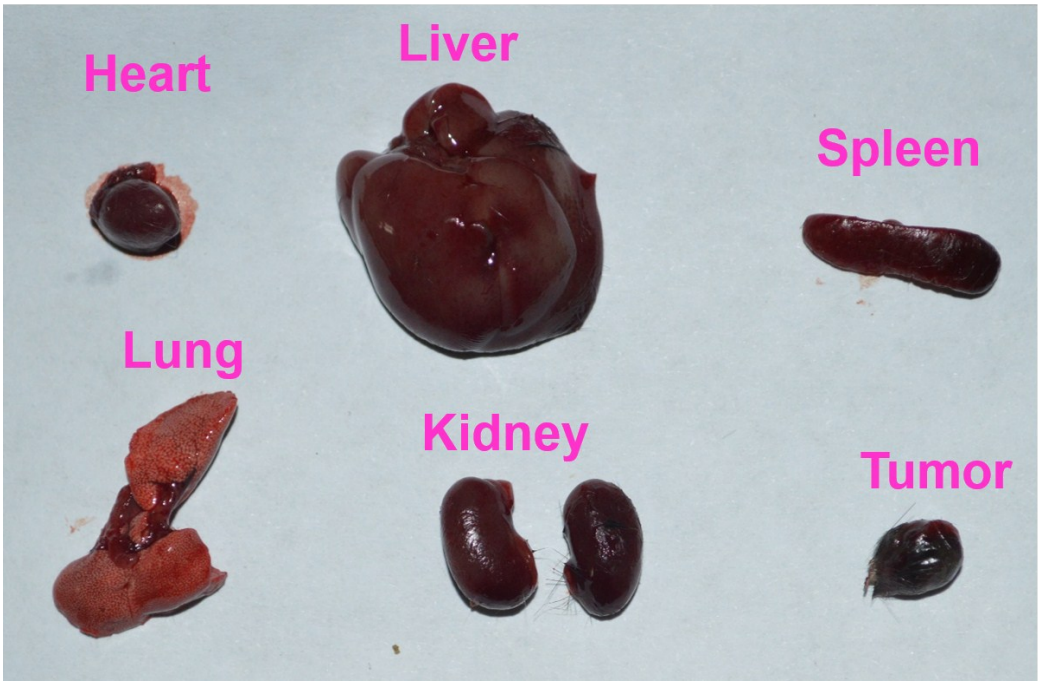


Fig. S9: The main internal organs and tumor of (WO+ICG)@PLGA nanoparticles loaded macrophages using tail vein injection group mice for 24 h.

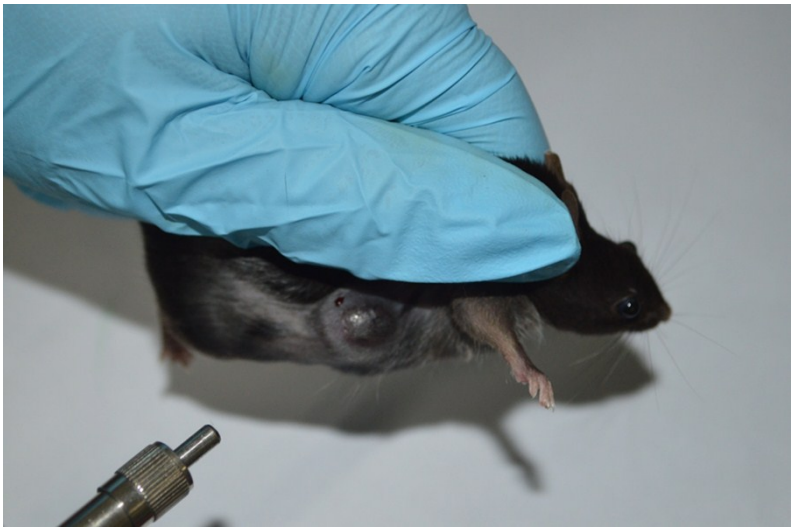

Fig. S10: The irradiation process using 808 nm NIR irradiating for the B16 subcutaneous tumor model in C57/B6 mice.

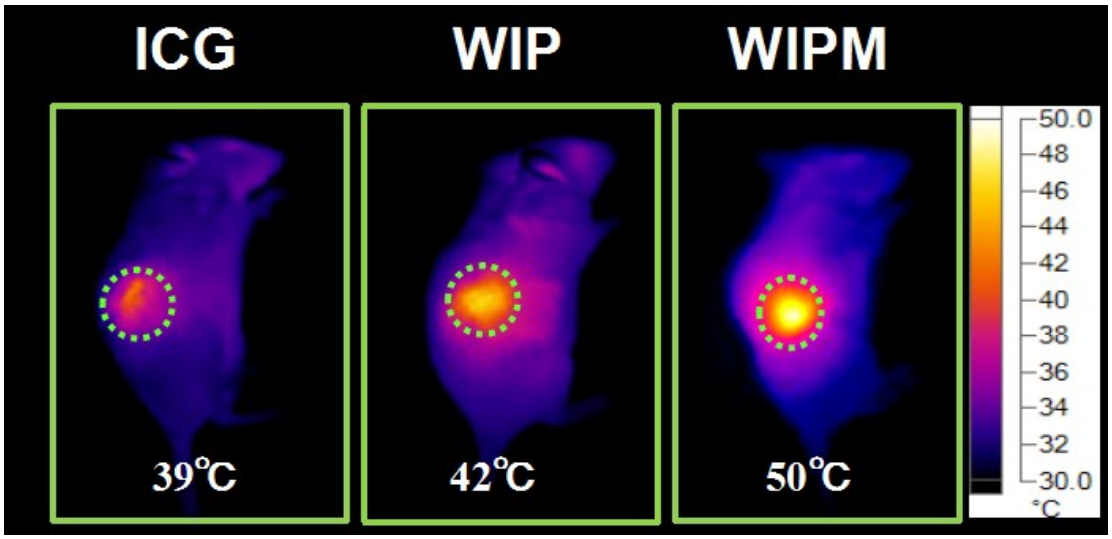


Fig. S11: The photo-thermal effects of different treatments *in vivo*, which received the 0.5 mg/ml ICG, 0.5 mg/ml (WO+ICG)@PLGA nanoparticles and 0.5 mg/ml (WO+ICG)@PLGA nanoparticles loaded macrophages using tail vein injection at $10^6$ Raw 264.7 cells after tail vein injection for 72 h, were detected by thermal imaging camera. The white number suggested the maximum temperature of 808 nm NIR light exposed region.

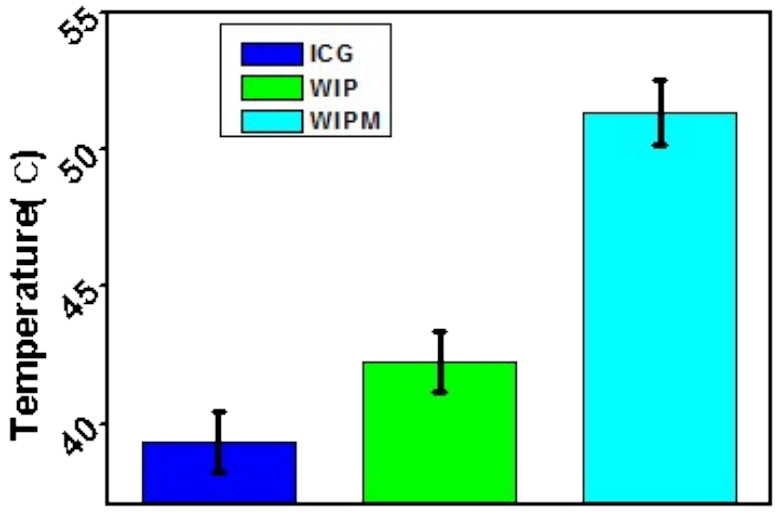


Fig. S12: The photo-thermal performance *in vivo* of different treatments after tail vein injection for 72 h.

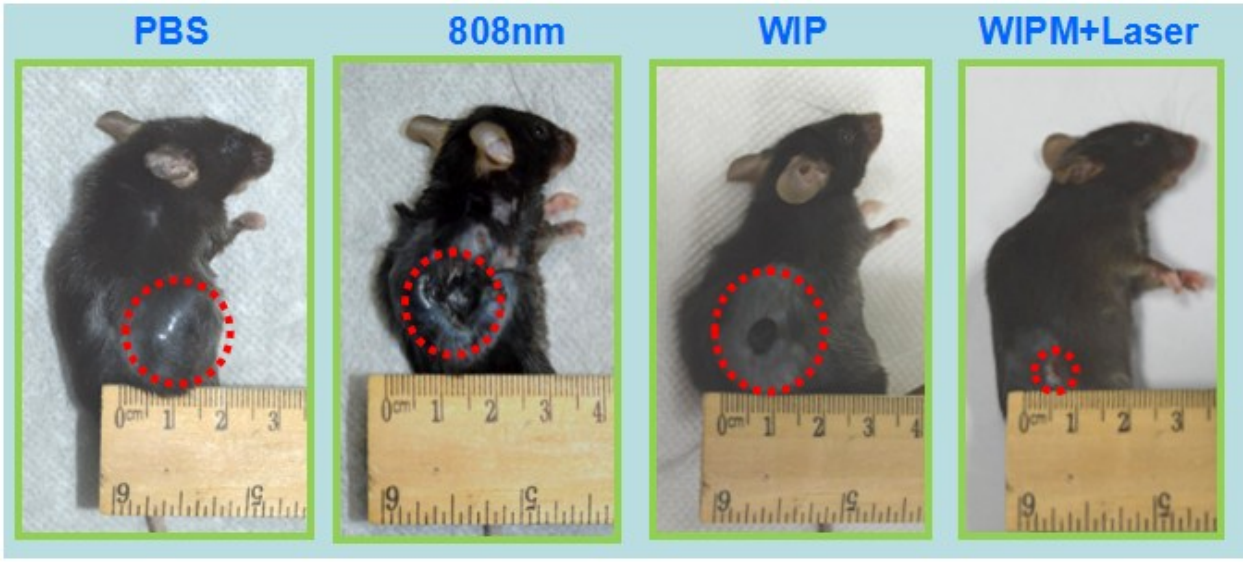


Fig. S13: In vivo tumor combined therapeutic efficiency of tumor size. There were four groups including PBS group, only 808 nm laser irradiation group, (WO+ICG)@PLGA nanoparticles without 808 nm irradiation group (WIP), and (WO+ICG)@PLGA nanoparticles loaded macrophages with 808 nm laser irradiation group (WIPM). The digital photographs were observed after experiment 15 days later.

**A**

```
data a;
input  t d g@@;
datalines;
2       1       1       3       1       2       1       1       3       12      1       4
6       1       1       6       1       2       5       1       3       15      1       4
7       1       1       9       1       2       6       1       3       19      1       4
10      1       1       11      1       2       9       1       3       24      1       4
15      1       1       16      1       2       15      1       3       30      1       4
;
proc lifetest plots=(s);
time t*d(0);
strata g;
ods rtf file='d:2.doc';
run;
ods rtf close;
```

**B**

| Test of Equality over Strata | | | |
|---|---|---|---|
| Test | Chi-Square | DF | Pr > Chi-Square |
| Log-Rank | 8.9714 | 3 | 0.0297 |

Fig. S14:The statistical significance of the survival curve is calculated by Survival Curve Comparison: Log-Rank Test. (A) The program of Statistics Analysis System. (B) The statistical results of survival curve. The p-values less than 0.05 was considered as statistically significant.

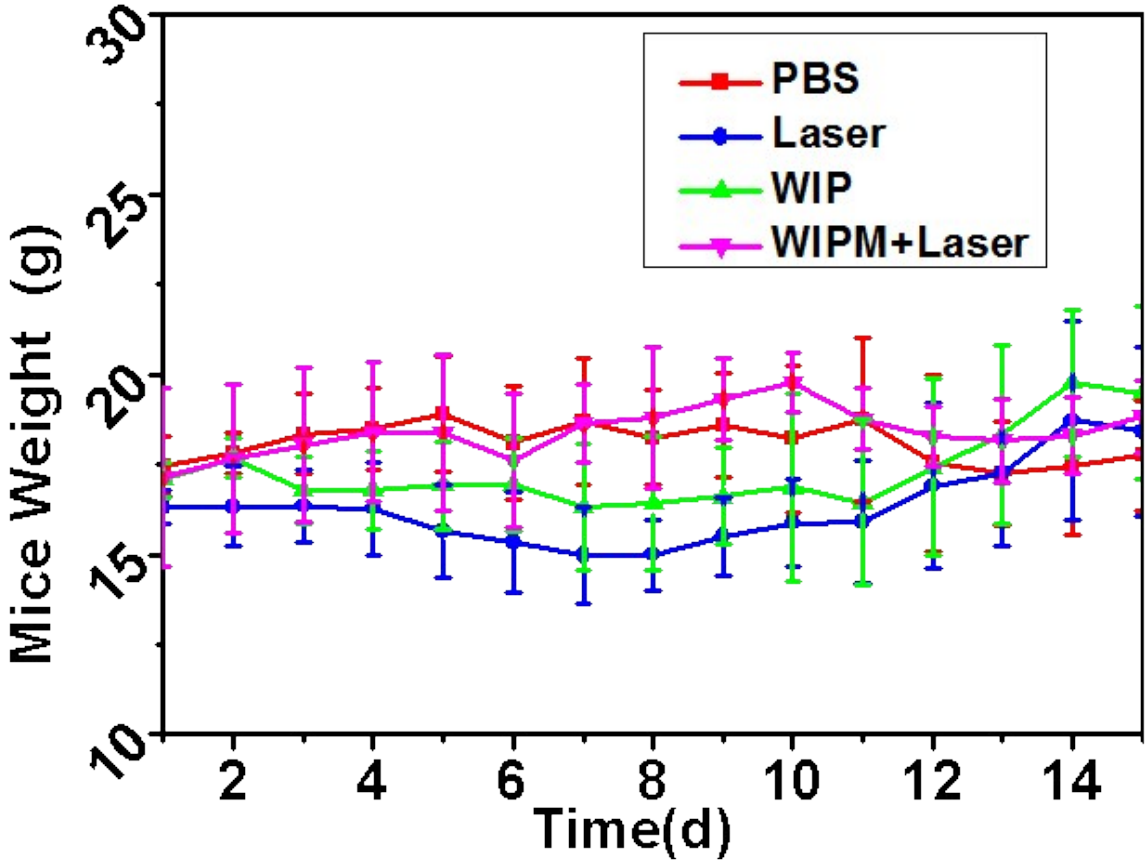


Fig. S15: The weight change in the B16 subcutaneous tumor model in C57/BL6 mice for treating with different ways within 15 days.